Crustal and upper mantle structure and the deep seismogenic environment in the source regions of the Lushan earthquake and the Wenchuan earthquake

ZHENG Yong[1], GE Can[1,2*], XIE ZuJun[1,2], YANG YingJie[3], XIONG Xiong[1] & HSU HouTze[1]

[1] *State Key Laboratory of Geodesy and Earth's Dynamics, Chinese Academy of Sciences, Wuhan 430077, China;*
[2] *College of Earth Sciences, University of Chinese Academy of Sciences, Beijing 100049, China;*
[3] *Australian Research Council Centre of Excellence for Core to Crust Fluid Systems/GEMOC, Department of Earth and Planetary Sciences, Macquarie University, North Ryde, New South Wales 2113, Australia*

Following the M_w7.9 Wenchuan earthquake, the M_w6.6 Lushan earthquake is another devastating earthquake that struck the Longmenshan Fault Zone (LFZ) and caused severe damages. In this study, we collected continuous broadband ambient noise seismic data and earthquake event data from Chinese provincial digital seismic network, and then utilized ambient noise tomography method and receiver function method to obtain high resolution shear wave velocity structure, crustal thickness, and Poisson ratio in the earthquake source region and its surroundings. Based on the tomography images and the receiver function results, we further analyzed the deep seismogenic environment of the LFZ and its neighborhood. We reveal three main findings: (1) There is big contrast of the shear wave velocities across the LFZ. (2) Both the Lushan earthquake and the Wenchuan earthquake occurred in the regions where crustal shear wave velocity and crustal thickness change dramatically. The rupture faults and the aftershock zones are also concentrated in the areas where the lateral gradients of crustal seismic wave speed and crustal thickness change significantly, and the focal depths of the earthquakes are concentrated in the transitional depths where shear wave velocities change dramatically from laterally uniform to laterally non-uniform. (3) The Wenchuan earthquake and its aftershocks occurred in low Poisson ratio region, while the Lushan earthquake sequences are located in high Poisson ratio zone. We proposed that the effect of the dramatic lateral variation of shear wave velocity, and the gravity potential energy differences caused by the big contrast in the topography and the crustal thickness across the LFZ may constitute the seismogenic environment for the strong earthquakes in the LFZ, and the Poisson ratio difference between the rocks in the south and north segments of the Longmenshan Fault zone may explain the 5 years delay of the occurrence of the Lushan earthquake than the Wenchuan earthquake.

Lushan earthquake, Wenchuan earthquake, receiver function, ambient noise tomography, deep seismogenic environment

On April 20, 2013, a M_w6.6 earthquake struck the south part of the Longmenshan Fault near Lushan county in Ya'an City [1, 2]. It is another strong earthquake which occurred in the LFZ following the Wenchuan earthquake occurring on May 12, 2008 [3]. This earthquake (hereafter called as Lushan earthquake) caused devastating damages to the source region. By April 24th, 2013, 196 people were killed, more than 10 thousand people were wounded and people in an area of 11500 square kilometers were threatened by this

*Corresponding author (email: gecan2008@gmail.com)

devastating earthquake.

The LFZ is situated at the boundary between the tectonically active Tibetan Plateau and the stable Yangtze Craton. The Yangtze Craton is an old and stable tectonic block; its crystallized basement was formed about 800 Ma ago. Since Cenozoic the Indian plate has collided with the Eurasian plate and caused about 1500–2000 km shortening between the two blocks [4, 5], which has dramatically affected the crustal structure in the west part of China [6, 7]. However, there is no obvious crustal shortening in the eastern boundary of the Tibetan Plateau, and massive crustal rocks may flow in the lower crustal channel, which thickens the crust and uplifts the Tibetan Plateau and its surroundings [8, 9]. When the low crustal flow is blocked by the strong Sichuan Basin, the rocks accumulate at the boundary between the Tibetan Plateau and the Sichuan Basin and form one of the steepest cliffs in the world [10, 11]. The average topography contrast between the two sides of the Longmenshan Mountain is about 3.5 km, and the crustal structure in this area has strong variations laterally and vertically.

Geoscientists attribute the tectonic activities, seismogenic environments and the distribution of earthquakes in the LFZ to the collision between the Indian Plate and the Eurasian Plate. However, more and more evidences show that the evolution process of crust is also controlled by the tectonic stresses from the far-field tectonic boundaries and the bottom of the lithosphere (external forces), and the regional gravity potential energy deviatoric stresses (internal forces) [12–16]. Studies on the Cordilleran Orogeny of the western United States and the southern Norwegian mountains show that the regional gravity potential energy plays key roles in the continental evolution [17]. And it is not necessary to invoke external forces arising from far-field plate kinematics or tractions at the base of the lithosphere to explain the present continental deformation characteristics [18]. The LFZ is located at the eastern boundary of the Tibetan Plateau, where the deviatoric stress generated by the difference of gravity potential energy is even larger than the driven force contributing to the mid-oceanic ridges surrounding the Indian Plate [19]. Thus the gravity potential energy should have strong effects on the evolution of the Tibetan Plateau [20] and the characteristics of seismicity [12]. Furthermore, even in the same tectonic settings, different rock properties can cause different deformation patterns under the same tectonic loadings. Therefore, only when most of the important factors, including external forces arising from far-field plate kinematics, tractions at the base of the lithosphere, regional gravity potential stresses, and rock properties are taken into consideration, the overall seismogenic mechanisms of the Lushan and Wenchuan earthquakes can be determined.

Having a precise crustal structure is critical to evaluate the gravity potential contrast [18, 21]. In addition, Poisson ratio, which is one important rock parameter, can be determined by measuring P and S wave velocities. Therefore, a study on precise crustal structure and Poisson ratio helps us to understand the properties of rupture faults and the geodynamic processes. With the rapid development of digital seismic network in this region [22, 23], it is possible now to obtain high resolution P, S and P_n wave velocity structures [24–31]. In this study, we applied the teleseismic receiver function method and the ambient noise tomography method to the broadband seismograms recorded by Chinese permanent broadband seismographs, and obtained high resolution crustal Poisson ratio, crustal thickness, and S wave velocity structures in the crust and the uppermost mantle in the Longmenshan region and its surroundings. These results provide a basis for further analyzing the deep seismogenic structures.

1 Method

In order to obtain crustal and uppermost mantle fine structure, we applied two methods in this study. Due to the importance of crustal thickness in understanding lateral variation of crust and surface wave inversion, we adopted teleseismic body wave receiver function method, which is sensitive to crustal thickness, to obtain crustal thickness and meanwhile also crustal passion ratio. Afterwards, we inversed crustal and uppermost mantle shear wave structure by ambient noise tomography method.

1.1 Teleseismic receiver function method

Teleseismic receiver function technique can efficiently remove source signals from seismic records and pick out structure information beneath the receiver [7, 32]. P wave receiver functions, which are calculated from teleseismic waves by deconvoluting vertical wave records from horizontal wave records, consist of a series of P-to-S converted arrivals and multiply arrivals (PpPs, PsPs+PpSs) generated from deep interfaces with different impedances. The most significant structure signal is from Moho interface. By analyzing the travel time of P-to-S converted arrivals and multiples, receiver function method is one of the most robust methods for estimating crustal thickness and average P-to-S velocity ratio. We used *H-κ* searching technique [33, 34] to obtain crustal thickness and average velocity ratio by stacking converted phases and multiples of receiver functions. Details on the computation of receiver functions and *H-κ* searching technique can be found elsewhere [33, 34]. In this study, we used a modified method to reduce stripe interference. Details of the modified method will be described in another paper and not elaborated in this paper. Because Poisson ratio directly reflects crustal elastic properties, we converted velocity ratio to Poisson ratio, using the following equation:

$$\sigma = \frac{1}{2}\{1 - [(V_p / V_s)^2 - 1]^{-1}\}. \tag{1}$$

1.2 Ambient noise tomography method

Because of strong attenuation and scatting of short period surface waves along teleseismic paths, it is difficult to pick up surface wave signals at short periods (<20 s) from teleseismic events. In addition, due to uneven distributions of earthquakes and uncertainties of earthquake source information, it is hard to obtain high resolution crustal structures using teleseismic surface wave tomography. In recent years, retrieving short and intermediate period surface waves from ambient noise by cross-correlating long time series of records between a pair of stations is getting more and more popular. Rather than using earthquake signals, ambient noise tomography uses ambient noise as signals. Thus ambient noise tomography is free from the requirement of earthquake source parameters. This method is highly capable to obtain high resolution tomographic results as long as seismic stations are dense and well distributed. This method has been proved an efficient method to construct short and moderate period's surface wave dispersion maps [35, 36]. In recent years, it has been widely used in tomography studies of Chinese continent and its surroundings [37–45]. Compared with traditional methods, high resolution surface wave images at short to intermediate periods resolved by ambient noise tomography provide more reliable constraints on crustal and uppermost mantle structures.

2 Data processing

We collected two years of continuous data from 2007 to 2009 recorded by 1171 broadband seismic stations distributed in China and surrounding areas. The distribution of stations is plotted in Figure 1. However, only those stations in the close areas of the Longmenshan Fault Zone, showed in Figure 1(a), are selected to form dense ray path coverage. Stations shown in Figure 1(b) are used in teleseismic re-

ceiver function study.

2.1 Receiver function data processing

We first selected teleseismic earthquake data with epicentral distances ranging from 30 to 95 degree, magnitudes > 5 and signal-to-noise ratios of P waves > 3. Then we used a time-domain iterative deconvolution approach to calculate the receiver functions. When processing low signal-to-noise ratio data, the time-domain approach is more robust than the water-level deconvolution [46]. We filtered the waveform data by adopting a Gauss lowpass filter with a corner frequency of 1.5 to reduce high frequency noise. Due to misorientation of azimuthal angles of horizontal components and polarization mislabeling of vertical components at some stations, we corrected the misorientation and polarization mislabeling based on a previous study [47]. At the meantime, we made data quality control by manually eliminating receiver functions with irregular waveform or abnormal large amplitude. In order to reduce the uncertainties derived from inaccurate search for velocities, we used average P wave velocity derived from Sun's East Asia P- and S-wave (SPEAS) crustal model [48, 49] as the search speed for each station. Figure 2 shows examples of H-κ search results and receiver functions at several stations close to the Wenchuan and Lushan earthquakes and aftershocks. Figure 2(a)–(c) represent the results of the stations in the north, where the crustal velocity ratio were lower than 1.73; Figure 2(d)–(f) represent southern stations, where the crustal velocity ratio is larger than 1.9. Stations in Figure 2(a), (b) and (d) are located in the Songpan-Ganzi block, where crustal thickness varies from 48 to 57 km; while the stations in Figure 2(c), 2(e) and (f) is located in the Sichuan Basin, where crustal thickness varies from 38 to 42 km.

2.2 Ambient noise data processing

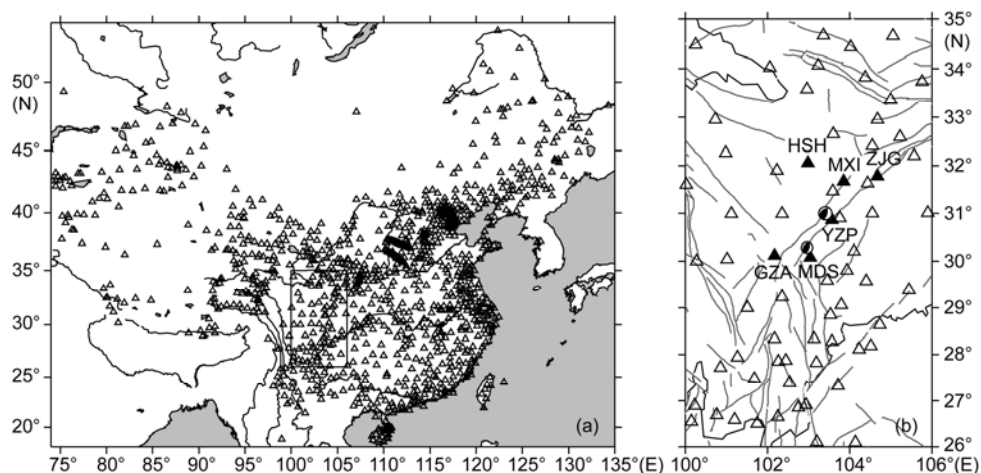Data processing procedures and quality control in this study

Figure 1 (a) Station distribution (triangles) used by ambient noise tomography; (b) stations (triangles) used in Teleseismic receiver Function study near the source. Solid triangles are the stations used in Figure 2; beach ball is the focal mechanism of Wenchuan earthquake [1] and Lushan earthquake [31].
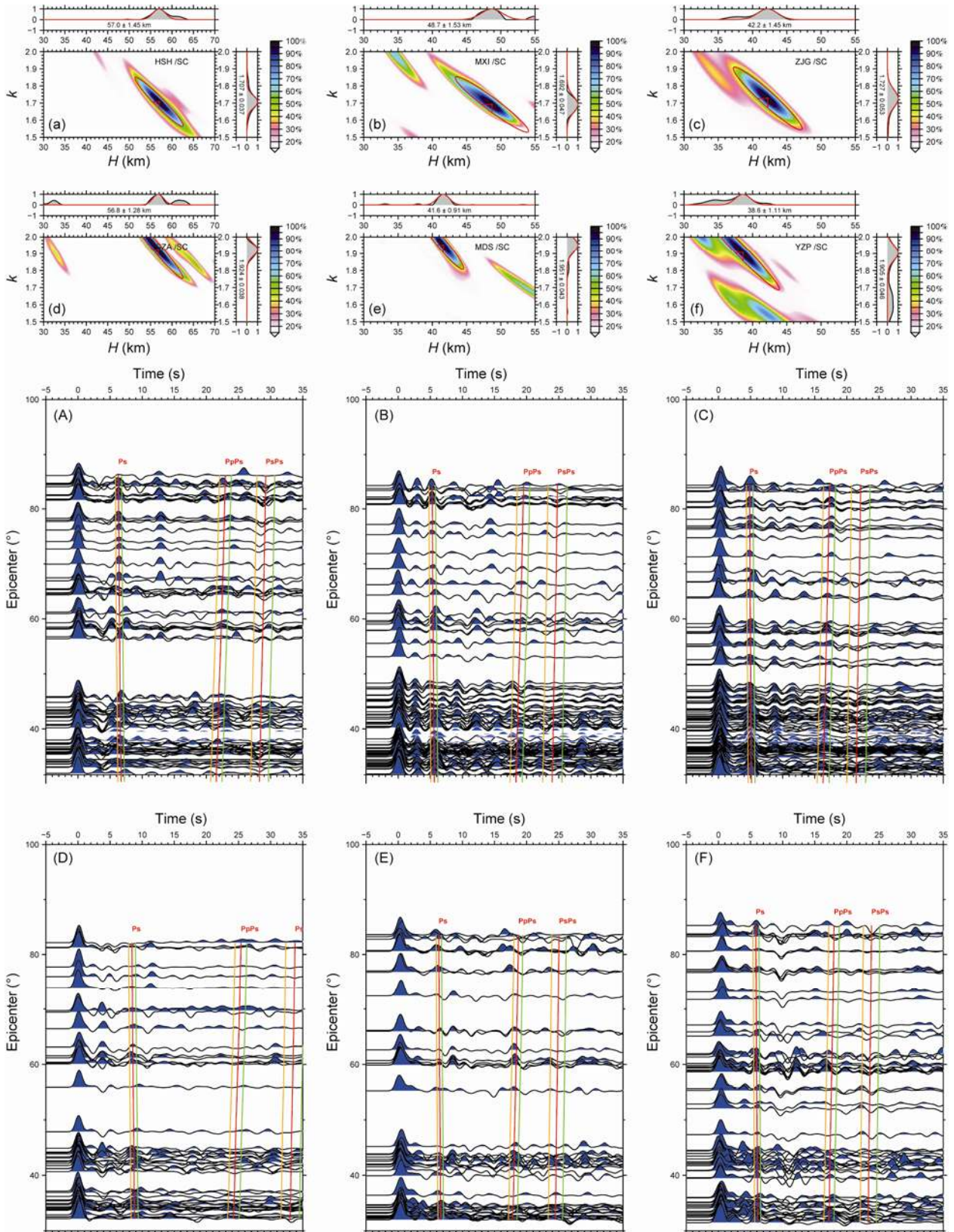
Figure 2   *H-κ* searching energy diagrams and the corresponding receiver function maps. Master maps of (a)–(f) are normalized energy diagrams by *H-κ* searching method. The gray curves in upper and left sides are searching energy varies with one variable when another fixed at optimal value and the red lines are the normalized Gaussian distribution function based on the corresponding search standard deviation. (A)–(F) are the corresponding receiver function map of (a)–(f). The red line marks the arrival time of converted wave (Ps) and multiples (PpPs, PsPs+PpSs) predicted by optimal value in energy diagram. Orange and green lines mark arrival time deviation caused by searching standard deviation.

are the same as Yang et al. [37, 38] and Zheng et al. [39, 40]. Because the data were collected from different networks, first we transformed the recording time to Greenwich Mean Time (GMT). Then, we removed instrument responses and preprocessed single station data. Daily cross-correlations were calculated between all pairs of stations and then over two years of cross-correlations were stacked to get high SNR ratio surface wave signals. Since only vertical component data were processed, the cross-correlation functions contain Rayleigh wave signals only. In order to keep our results stable, both group and phase velocities were measured by the automated frequency-time analysis method [50, 51]. We only chose high SNR dispersion measurements with inter-station path length larger than 3 wavelengths, and then used the surface wave tomography method developed by Barmin et al. [15] to produce Rayleigh wave group and phase speed maps at different periods. Figure 3 shows the ray path coverage and phase velocity resolution of different periods in surface wave tomography study. Based on the group and the phase velocity maps (Figure 4), we constructed a 3-D model of the crustal and uppermost mantle structure by a Monte Carlo inversion [53, 54] in the area where the lateral resolution of surface wave dispersion maps is less than 200 km.

3 Results and analysis

3.1 Crustal thickness and Poisson ratio

To illustrate the crustal structure in and around the source region of the Lushan earthquake, we constructed crustal thickness and Poisson ratio maps from H-κ measurements of each station (Figure 5, Appendix 1, www.springerlink.com/scp). In this paper, we used the adjustable tension continuous curvature surface interpolation algorithm to get the interpolation value $z(x,y)$ by solving the equation:

$$(1-T)\times L(L(z))+T\times L(z)=0, \qquad (2)$$

where L is the Laplace operator, T is the tension coefficient, $T = 0$ gives the minimum curvature solution; $T = 1$ gives the Laplace harmonic surface solution. Generally, $T = 0.35$ is often used for the steep topography data. Crustal thickness and Poisson ratio maps (Figure 5) exhibit drastic variations across the Longmenshan. Average crustal thickness of the Sichuan Basin is around 42 km, close to the average thickness 41.5 km of cratonic regions [55]. While in the Longmenshan region, crustal thickness increases to thicker than 50 km rapidly. In the south part of the Songpan-Ganzi block, the crustal thickness is thickened to 64–68 km, which is much thicker than the average crustal thickness of global orogenic belts (46.3 km) [55]. Our result is consistent with the result of deep seismic reflection study, in which the crustal thickness of the Sichuan Basin is 43 km and the

crustal thickness of eastern Tibetan plateau is 63 km [56]. Poisson ratio map exhibits low Poisson ratio (<0.25) in the north and central segments of the LFZ, but high value (>0.29) in the south segment. Results from another array across the south segment of the Longmenshan faults along 30°N indicate that there is an abnormally high Poisson ratio region between 102°E and 103°E, which is consistent with our work [57].

3.2 Crustal and upper-mantle S velocity structure

We constructed 3D shear wave velocity structure of crust and uppermost mantle from the inversion of group and the phase velocity dispersion maps obtained by ambient noise tomography (Figure 6, Appendix 2, www.springerlink.com/scp). At shallow depths such as 5 km, shear velocities are low in the Sichuan Basin and high in the eastern Tibet. However, the pattern of lateral velocity variation changes gradually with depths increasing from 10 to 15 km. Below ~20 km, the pattern of velocity variations is completely reversed. The low velocities in shallow depths of the Sichuan Basin are mainly due to the thick sedimentary layers. The high velocities in the middle and lower crust of the Sichuan Basin mainly reflect the low temperate and high rigidness of the Sichuan Basin as the western part of the stable Yangtze Craton, while the strong velocity contrasts across the LFZ depths of 50 to 70 km mainly reflect the variation of crustal thickness with the lower crust still present in the Eastern Tibet but the uppermost mantle present in the Sichuan Basin at this range of depths. Generally speaking, for rocks comprised of similar minerals, high speed anomalies correspond to high density and strong rigidness, which is probably the reason why the high velocity Sichuan Basin remains strong and stable. From the velocity maps, we found that both of the Lushan earthquake and the Wenchuan earthquake occurred in the area with dramatic velocity changes. These two earthquakes occurred in the depth of 13–17 km, where is the transitional depth of seismic velocity in the both sides of the LFZ (Figure 7).

Ambient noise tomography is not sensitive to the velocity interfaces, but sensitive to the absolute velocity values. On the contrary, the teleseismic receiver function method is more sensitive to the velocity interfaces, but less sensitive to absolute velocities. The resolutions of these two methods are different as well. The resolution of ambient noise tomography increases with increasing ray density. In this work the lateral resolution reaches ~50 to 80 km. The teleseismic receiver function method obtains an average structure beneath each station, and the lateral resolution increases with the increasing station density. In this paper the resolution of the receive function method reaches about 100 km. The conformity of the crustal structures in terms of lateral variations obtained by these two independent methods suggests that the results from the two methods are reliable to some extent.
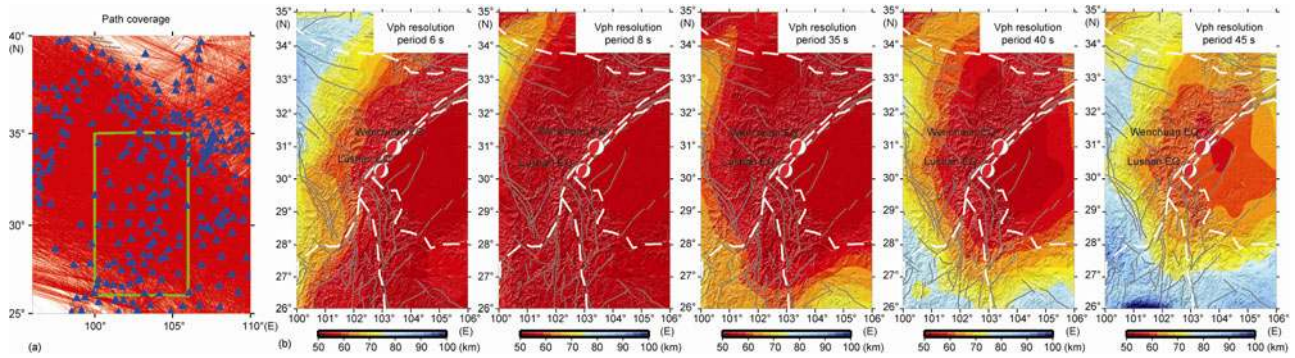
Figure 3   Ray path coverage of 45 s period phase velocity (a) and phase velocity resolution (b) maps of different periods in study area. Figirue (b) shows phase velocity resolution maps of period of 6, 8, 35, 40 and 45 s in study area, whose resolution is around 50–80 km, the resolution between 8 and 35 s period is up to 50 km. The group velocity resolution maps are similar.
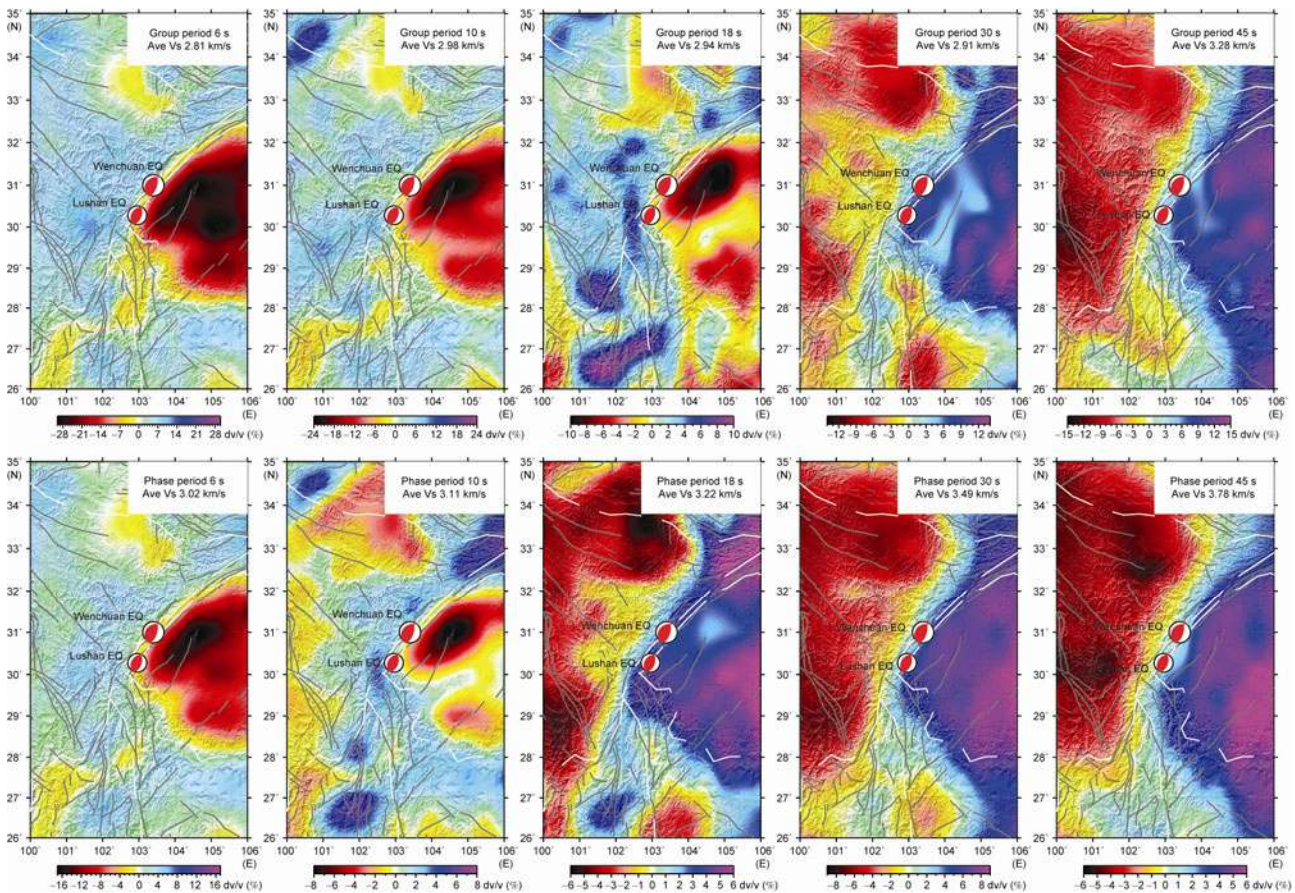

Figure 4   Phase velocity and group velocity maps in study area during the period of 6, 8, 35, 40 and 45 s. The white dotted are the boundary line of the main tectonic blocks; the gray lines are the active fault in study area [52]; beach balls are the focal mechanisms of Wunchuan earthquake and Lushan earthquake.

4   Relationship between the seismogenic structures of the Wenchuan and the Lushan earthquakes

Based on the analysis of the results of crustal structure in this work, there are some similarities in seismogenic environment between the Lushan earthquake and the Wenchuan earthquake. Both of them occurred in the regions where the topography, crustal thickness and velocity structure change dramatically. The elevation of the area decreases from 4 to 0.5 km and the crust thins quickly from ~60 to ~40 km over a short distance of 150 km across the LFZ. The velocity structure shows that the crustal layers with different velocities are quite flat in the Sichuan Basin, while the middle crust with a shear velocity of ~3.4–3.5 km/s in the Songpan-Ganzi
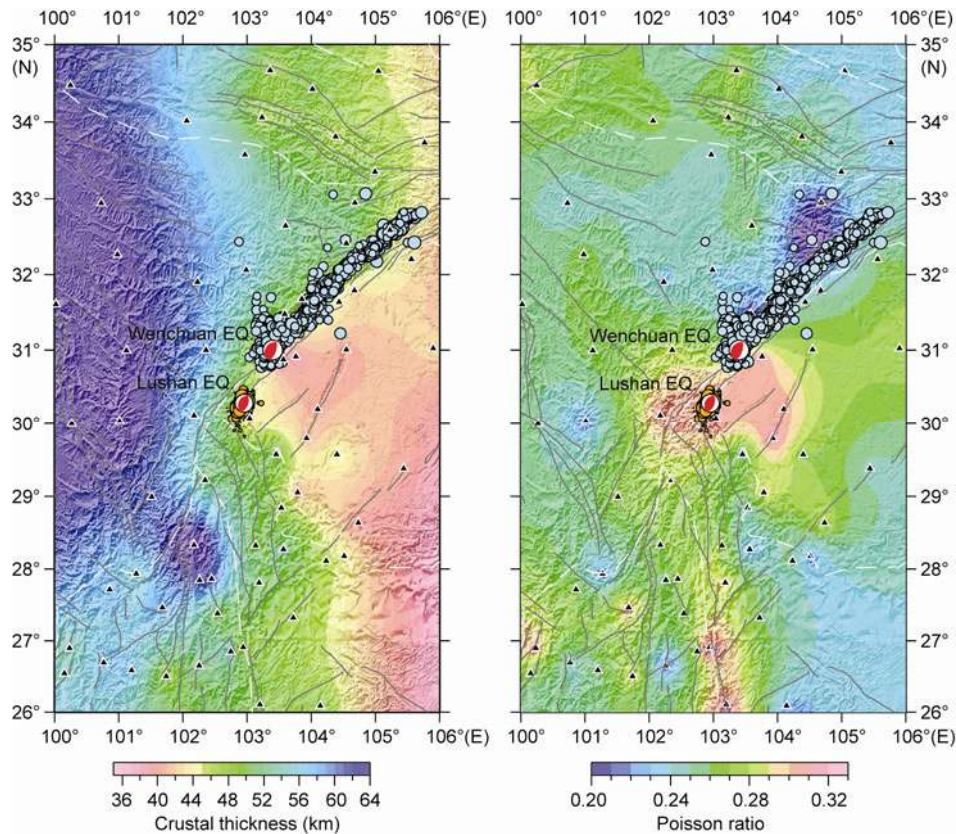
Figure 5 Crustal thickness map and Poisson ratio map achieved by receiver function study. The black triangles represent the station location. Beach balls are Wunchuan earthquake and Lushan earthquake. Light blue circles represent the aftershock distribution of wenchuan earthquake. Orange circles represent the aftershocks distribution of Lushan earthquake. Lines in this figure are consistent with Figure 4.

block to the west of Longmenshan thickens significantly towards west. The same characteristics are also observed in P-wave velocity structure in these regions [25]. The velocities are close to each other at 10 km depth at both sides of the LFZ, but the velocities in the Sichuan Basin gradually gets higher than those in the Songpan-Ganzi block at the depths greater than 15 km, reflecting that the east side of the LFZ is stronger and more stable than the west side. The variation of velocity contrast with depth in the horizontal direction is consistent with the seismogenic depth of the Wenchuan earthquake and the Lushan earthquake. In other words, the earthquakes occurred in the transition depth of seismic velocity from horizontally uniform to non-uniform.

However, the seismogenic environments of the Lushan earthquake and the Wenchuan earthquake also have some differences. The Wenchuan earthquake occurred in the area with an average Poisson ratio as low as ~0.27, and its aftershocks are mainly concentrated in the middle and north segments of the Longmenshan Fault Zone where average Poisson ratio is lower. On the contrary, the Lushan earthquake and its aftershocks mainly occurred in the area with high Poisson ratio (Figure 5). The 3D Poisson ratio model and the rupture fault constructed by P and S wave tomography exhibit that the rupture of the Wenchuan earthquake initiated at a low Poisson ratio region and terminated at the

high Poisson ratio region, and then restarted in a low Poisson ratio region [58]. Besides, most of the Wenchuan aftershocks are also located in the areas with low seismic velocities and low Poisson ratio [59]. Soon after the occurrence of the Wenchuan earthquake, Shan et al. [60] calculated Coulomb Failure Stress (CFS). They find that the CFS increase exceeds the threshold of Coulomb stress triggering not only in the north segment of the LFZ but also in most of the areas close to the epicenter of the Lushan earthquake by more than 0.02 MPa, with the maximum increase reaching up to 0.0749 MPa, which is also larger than the threshold of 0.01 MPa [60]. However, the aftershocks of the Wenchuan earthquake didn't occur in the south segment of the Longmenshan Fault Zone where the CFS increases exceed the threshold until the Lushan earthquake happened in 2013 5 years later than the occurrence of the Wenchuan earthquake. Is there any relationship between the temporal-spatial distribution of earthquakes and the Poisson ration pattern in the LFZ?

A number of factors affect Poisson ratio of rocks, such as temperature, pressure, crack porosity, composition, and so on. Based on laboratory measurements, the most important factors that affect Poisson ratio of common plutonic igneous rocks and metamorphic rocks are rock composition and molten status. When pressure is up to 100–200 MPa (equiv-
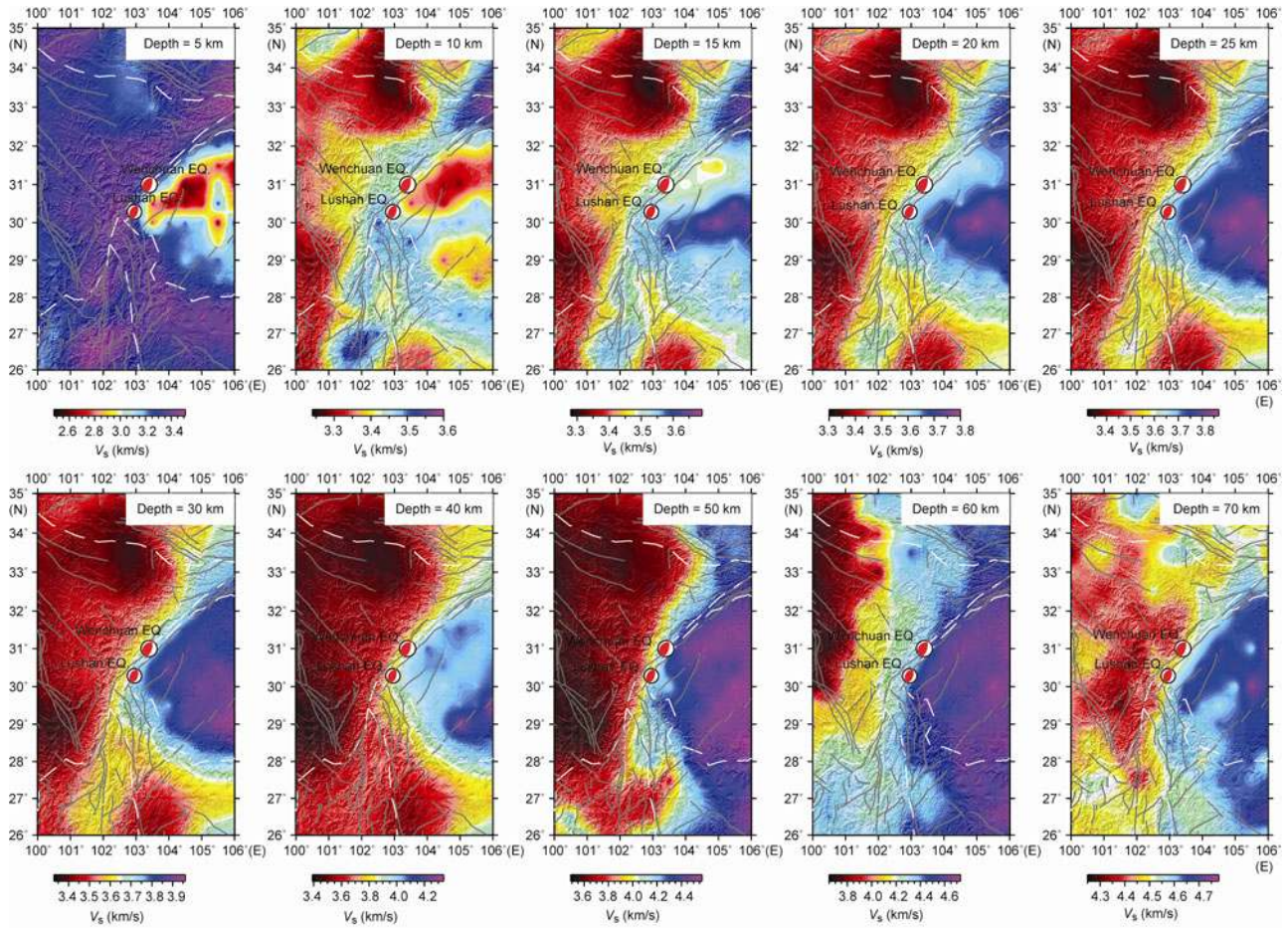
Figure 6   S velocity map at different depth achieved by ambient noise tomography. Beach balls and lines in this figure are consistent with Figure 4.
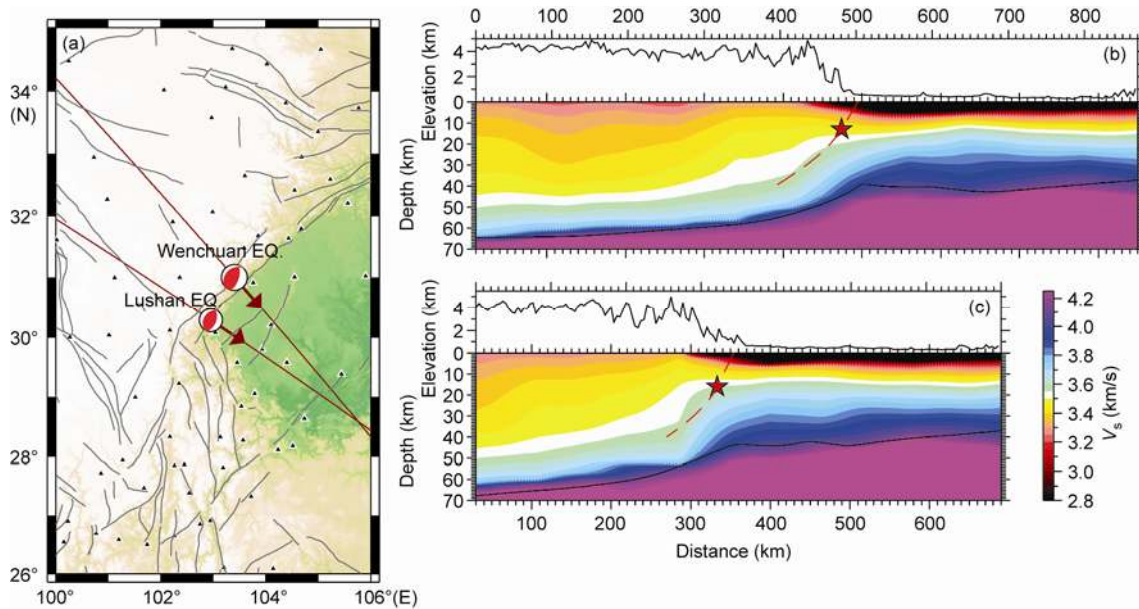

Figure 7   S velocity profiles across the longmen faults zone. (a) Profiles location across Wunchuan and Lushan earthquake. Profile directions are perpendicular to the strike direction of two earthquakes. (b) S velocity profile across Wenchuan earthquake; Top thin black line is the elevation variance at profile surface; bottom thick black line represent crustal thickness achieved by receiver function study; red thin line represent the suppositional inclined fault surface. (c) Same as (b) but structure profile across Lushan earthquake.

alent to crust hydrostatic pressure at ~7.5 to 15 km depths), cracks in most rocks close and thus temperature and pressure effects become insignificant. In that case, velocity ratio and Poisson ratio of rocks are mainly controlled by rock compositions [61]. Quartzand Plagioclase are two major diagenetic minerals. Quartz is characterized by low Poisson ratio of 0.09, while Plagioclase is characterized by high Poisson ratio of 3.0. In laboratory studies, a linear correlation of increasing Poisson ratio (from 0.232 to 0.304) with decreasing SiO_2 content is observed for rocks with 55 wt % to 75 wt% SiO_2. Poisson ratio increases from 0.24 to 0.29 as granitic rocks transform to gabbro with the increasing composition of Plagioclase and then decreases to 0.25 in dunite [61] with the decreasing composition of plagioclase. On the other hand, the presence of partial melt in rocks has significant influence on Poisson ratio. Because Poisson ratio in ideal fluid is as high as 0.5, hot fluid and partial melt rock would decrease rock shear modulus, and therefore increase velocity ratio and Poisson ratio significantly. Taking granitic rocks for instance, 5% partly melt content would result in velocity ratio as high as 1.9 and Poisson ratio up to 0.31. Thus, for those regions where Poisson ratio is too high to be matched by changing rock composition, the crustal rocks are very likely to be partially melted.

Therefore, we suggest that in the central to north segments of the LFZ, rocks may contain higher content of Quartzite and lower content of Plagioclase; while in the south segment of the LFZ, rocks have higher content of Plagioclase and lower content of Quartzite, and may even be partial melted. Laboratory studies prove that quartzite and granitic rocks are characterized by high friction coefficient (~0.65), which would decrease slightly with presence of a small amount of water; while pyroxene, plagioclase and gabbro are characterized by higher friction coefficient (~0.75), and are insensitive to the presence of a small amount of water and high temperature environment [62]. The consequence of different chemical composition and status of rocks between the south and the north segments of the LFZ is that under the same tectonic loadings, higher Poisson ratio rocks in the south segment of LFZ deform easily in lateral direction so that it can absorb more strain energy, while the higher friction coefficient of those rocks makes them harder to rupture along the fault plane. Based the rock properties we thus speculate that higher Poisson ratio and higher friction coefficient of rocks in the south LFZ than in the south and the central LFZ is the main reason why there is dramatic difference in seismogenic processes between the north/central segments and the south segments during the Wenchuan earthquake. After five years of strain accumulation and effects of the co-seismic and post-seismic Coulomb stress induced by the Wenchuan earthquake [60, 63], the stresses acting on the rocks in south segment exceeded the threshold value and generated the Lushan earthquake.

5　Conclusions

We have revealed detailed features of crustal structure of the Longmenshan Faults Zone and its adjacent area using two independent methods: teleseismic receiver function and ambient noise tomography. The analysis results indicate that both the Wenchuan earthquake and the Lushan earthquake occurred in areas where both crustal velocity and crustal thickness vary dramatically. Large gravitational potential contrast is caused by the huge topography difference and the variation of crustal thickness across the LFZ. The large gravity potential stress and the strong lateral changes of shear wave velocity from the Sichuan Basin to the west Tibetan Plateau constitute the seismogenic environment of the Wenchuan and Lushan earthquakes. However, the seismogenic structures of these two strong earthquakes have some differences. The Lushan earthquake occurred in the area with high crustal average Poisson ratio, while the Wenchuan earthquake and its aftershock sequence mainly occurred in low Poisson ratio areas. Since Poisson ratio is related to crustal rock composition and strength, Poisson ratio may be the key to solve the puzzle why the Wenchuan earthquake and its aftershocks mainly ruptured northward, and left a nonruptured zone in the south segment of the LFZ. With the accumulation of tectonic stress and the Coulomb stress generated by the co- and post-seismic effects of the Wenchuan earthquake, the south segment broke eventually and the Lushan earthquake occurred. Considering the complexities of seismogenic mechanism of the intraplate earthquakes, the relationship between the seismicity and the crustal rock properties in different segments of the Longmen faults is needed to be further studied.

1　Xie Z J, Jin B K, Zheng Y, et al. Source parameters inversion of the 2013 Lushan earthquake by combining teleseismic waveforms and local seismograms. Sci China Earth Sci, 2013, doi: 10.1007/s11430-013-4640-3

2　Liu C L, Zheng Y, Ge C, et al. Rupture Process of the M_s7.0 Lushan Earthquake, 2013. Sci China Earth Sci, 2013, doi: 10.1007/s11430-013-4639-9

3　Zhang P Z, Xu X W, Wen X Z, et al. Slip rates and recurrence inter-

vals of the Longmen Shan active fault zone, and tectonic implications for the mechanism of the May 12 Wenchuan earthquake, 2008, Sichuan, China (in Chinese). Chin J Geophys, 2008, 51: 1066–1073

4 Yin A, Harrison T M. Geological evolution of the Himalayan-Tibetan Orogen. Annu Rev Earth Planet Sci, 2000, 28: 211–280

5 Yi Z, Huang B, Chen J, et al. Paleomagnetism of early Paleogene marine sediments in southern Tibet, China: Implications to onset of the India-Asia collision and size of Greater India. Earth Planet Sci Lett, 2011, 309: 153–165

6 Wu Q J, Zeng R S, Zhao W J. The upper mantle structure of the Tibetan Plateau and its implication for the continent-continent collision. Sci China Ser D-Earth Sci, 2005, 48: 1158–1164

7 Wu Q J, Zeng R S. The Crustal structure of Qinghai-Xizang Plateau inferred from broadband teleseismic waveform (in Chinese). Chin J Geophys, 1998, 41: 669–679

8 Clark M K, Royden L H. Topographic ooze: Building the eastern margin of Tibet by lower crustal flow. Geology, 2000, 28: 703–706

9 Royden L H, Burchfiel B C, van der Hilst R D. The geological evolution of the Tibetan Plateau. Science, 2008, 321: 1054–1058

10 Zhang Z, Yuan X, Chen Y, et al. Seismic signature of the collision between the east Tibetan escape flow and the Sichuan Basin. Earth Planet Sci Lett, 2010, 292: 254–264

11 Zhang Z, Wang Y, Chen Y, et al. Crustal structure across Longmenshan fault belt from passive source seismic profiling. Geophys Res Lett, 2009, 36: L17310, doi: 10.1029/2009GL039580

12 England P, Molnar P. Active deformation of Asia: From kinematics to dynamics. Science, 1997, 278: 647–650

13 Rey P, Vanderhaeghe O, Teyssier C. Gravitational collapse of the continental crust: Definition, regimes and modes. Tectonophysics, 2001, 342: 435–449

14 Bendick R, Flesch L. Reconciling lithospheric deformation and lower crustal flow beneath central Tibet. Geology, 2007, 35: 895–898

15 Barmin M P, Ritzwoller M H, Levshin A L. A fast and reliable method for surface wave tomography. Pure Appl Geophy, 2001, 158: 1351–1375

16 Ghosh A, Holt W E, Flesch L M. Contribution of gravitational potential energy differences to the global stress field. Geophys J Int, 2009, 179: 787–812

17 Pascal C, Cloetingh S A P L. Gravitational potential stresses and stress field of passive continental margins: Insights from the south-Norway shelf. Earth Planet Sci Lett, 2009, 277: 464–473

18 Jones C H, Unruh J R, Sonder L J. The role of gravitational potential energy in active deformation in the southwestern United States. Nature, 1996, 381: 37–41

19 Ghosh A, Holt W E, Flesch L M, et al. Gravitational potential energy of the Tibetan Plateau and the forces driving the Indian plate. Geology, 2006, 34: 321–324

20 Hodges K V, Hurtado J M, Whipple K X. Southward extrusion of Tibetan crust and its effect on Himalayan tectonics. Tectonics, 2001, 20: 799–809

21 Naliboff J B, Lithgow-Bertelloni C, Ruff L J, et al. The effects of lithospheric thickness and density structure on Earth's stress field. Geophys J Int, 2012, 188: 1–17

22 Zheng X F, Ouyang B, Zhang D N, et al. Technical system construction of Data Backup Centre for China Seismograph Network and the data support to researches on the Wenchuan earthquake (in Chinese). Chin J Geophys, 2009, 52: 1412–1217

23 Zheng X F, Yao Z X, Liang J H, et al. The role played and opportunities provided by IGP DMC of China National Seismic Network in Wenchuan earthquake disaster relief and researches. Bull Amer Meteorol Soc, 2010, 100: 2866–2872

24 Li Z W, Ni S D, Hao T Y, et al. Uppermost mantle structure of the eastern margin of the Tibetan plateau from interstation Pn traveltime difference tomography. Earth Planet Sci Lett, 2012, 335-336: 195–205

25 Li Z W, Xu Y, Huang R Q, et al. Crustal P-wave velocity structure of the Longmenshan region and its tectonic implications for the 2008 Wenchuan earthquake. Sci China Earth Sci, 2011, 54: 1386–1393

26 Xu Y, Li Z W, Huang R, et al. Seismic structure of the Longmen Shan region from S-wave tomography and its relationship with the

Wenchuan M_s8.0 earthquake on 12 May 2008, sourthwestern China. Geophys Res Lett, 2010, 37: L02304, doi: 10.1029/2009GL041835

27 Li C, van der Hilst R D, Toksöz M N. Constraining P-wave velocity variations in the upper mantle beneath Southeast Asia. Physics Earth Planet Int, 2006, 154: 180–195

28 Li C, van der Hilst R D, Engdahl E R, et al. A new global model for P wave speed variations in Earth's mantle. Geochem Geophys Geosyst, 2008, 9: Q05018, doi: 10.1029/2007GC001806

29 Bai Z, Tian X, Tian Y. Upper mantle P-wave tomography across the Longmenshan fault belt from passive-source seismic observations along Aba-Longquanshan profile. J Asian Earth Sci, 2011, 40: 873–882

30 Liang C, Song X, Huang J. Tomographic inversion of Pn travel times in China. J Geophys Res, 2004, 109: B11304

31 Zhang P Z, Wen X, Shen Z K, et al. Oblique, high-angle, listric-reverse faulting and associated development of strain: The Wenchuan earthquake of May 12, 2008, Sichuan, China. Annu Rev Earth Planet Sci, 2010, 38: 353–382

32 Langston C A. Structure under Mount Rainier, Washington, inferred from teleseismic body waves. J Geophys Res, 1979, 84: 4749–4762

33 Zhu L, Kanamori H. Moho depth variation in southern California from teleseismic receiver functions. J Geophys Res, 2000, 105: 2969–2980

34 Ge C, Zheng Y, Xiong X. Study of crustal thickness and Poisson ratio of the North China Craton (in Chinese). Chin J Geophys, 2001, 54: 2538–2548

35 Sabra K G, Gerstoft P, Roux P, et al. Surface wave tomography from microseisms in Southern California. Geophys Res Lett, 2005, 32: L14311, doi: 10.1029/2005GL023155

36 Shapiro N M, Campillo M, Stehly L, et al. High-resolution surface-wave tomography from ambient seismic noise. Science, 2005, 307: 1615–1618

37 Yang Y, Ritzwoller M H, Zheng Y, et al. A synoptic view of the distribution and connectivity of the mid-crustal low velocity zone beneath Tibet. J Geophys Res, 2012, 117: B04303, doi: 10.1029/2011JB008810

38 Yang Y, Zheng Y, Chen J, et al. Rayleigh wave phase velocity maps of Tibet and the surrounding regions from ambient seismic noise tomography. Geochem Geophys Geosystem, 2010, 11: Q08010, doi: 10.1029/2010GC003119

39 Zheng Y, Shen W, Zhou L, et al. Crust and uppermost mantle beneath the North China Craton, northeastern China, and the Sea of Japan from ambient noise tomography. J Geophys Res, 2011, 116, B12312, doi: 10.1029/2011JB008637

40 Zheng Y, Yang Y, Ritzwoller M H, et al. Crustal structure of the northeastern Tibetan plateau, the Ordos block and the Sichuan basin from ambient noise tomography. Earthquake Sci, 2010, 23: 465–476

41 Zhou L, Xie J, Shen W, et al. The structure of the crust and uppermost mantle beneath South China from ambient noise and earthquake tomography. Geophys J Int, 2012, 189: 1565–1583

42 Luo Y, Xu Y, Yang Y. Crustal structure beneath the Dabie orogenic belt from ambient noise tomography. Earth Planet Sci Lett, 2012, 313: 12–22

43 Yao H, Campman X, de Hoop M V, et al. Estimation of surface wave Green's functions from correlation of direct waves, coda waves, and ambient noise in SE Tibet. Phys Earth Planet Int, 2009, 177: 1–11

44 Yao H, van der Hilst R D. Analysis of ambient noise energy distribution and phase velocity bias in ambient noise tomography, with application to SE Tibet. Geophys J Int, 2009, 179: 1113–1132

45 Yao H, Beghein C, van der Hilst R D. Surface wave array tomography in SE Tibet from ambient seismic noise and two-station analysis–II. Crustal and upper-mantle structure. Geophys J Int, 2008, 173: 205–219

46 Ligorría J P, Ammon C J. Iterative deconvolution and receiver-function estimation. Bull Seismol Soc Amer, 1999, 89: 1395–1400

47 Niu F, Li J. Component azimuths of the CEArray stations estimated from P-wave particle motion. Earthquake Sci, 2011, 24: 3–13

48 Sun Y, Toksöz M N. Crustal structure of China and surrounding regions from P wave traveltime tomography. J Geophys Res, 2006, 111:

B03310, doi: 10.1029/2005JB003962

49 Sun Y, Li X, Kuleli S, et al. Adaptive moving window method for 3D P-velocity tomography and its application in China. Bull Seismol Soc Amer, 2004, 94: 740–746

50 Bensen G D, Ritzwoller M H, Barmin M P, et al. Processing seismic ambient noise data to obtain reliable broad-band surface wave dispersion measurements. Geophys J Int, 2007, 169: 1239–1260

51 Lin F C, Moschetti M P, Ritzwoller M H. Surface wave tomography of the western United States from ambient seismic noise: Rayleigh and Love wave phase velocity maps. Geophys J Int, 2008, 173: 281–298

52 Zhang P Z, Deng Q D, Zhang G M, et al. Active tectonic blocks and strong earthquake in the continent of China. Sci China Ser D-Earth Sci, 2003, 46: 13–24

53 Shen W, Ritzwoller M H, Schulte-Pelkum V, et al. Joint inversion of surface wave dispersion and receiver functions: A Bayesian Monte-Carlo approach. Geophys J Int, 2013, 192: 807–836

54 Shen W, Ritzwoller M H, Schulte-Pelkum V. A 3-D model of the crust and uppermost mantle beneath the Central and Western US by joint inversion of receiver functions and surface wave dispersion. J Geophys Res, 2013, 118: 262–276

55 Christensen N I, Mooney W D. Seismic velocity structure and composition of the continental crust: A global view. J Geophys Res, 1995, 100: 9761–9788

56 Wang C Y, Han W B, Wu J P, et al. Crustal structure beneath the eastern margin of the Tibetan Plateau and its tectonic implications. J Geophys Res, 2007, 112: B07307, doi: 10.1029/2005JB003873

57 Wang C Y, Lou H, Lü Z Y, et al. S-wave crustal and upper mantle's velocity structure in the eastern Tibetan Plateau—Deep environment of lower crustal flow. Sci China Ser D-Earth Sci, 2008, 51: 263–274

58 Wang Z, Fukao Y, Pei S. Structural control of rupturing of the Mw7.9 2008 Wenchuan Earthquake, China. Earth Planet Sci Lett, 2009, 279: 131–138

59 Lei J, Zhao D. Structural heterogeneity of the Longmenshan fault zone and the mechanism of the 2008 Wenchuan earthquake (M_s8.0). Geochem Geophys Geosyst, 2009, 10: Q10010, doi: 10.1029/2009GC002590

60 Shan B, Xiong X, Zheng Y, et al. Stress changes on major faults caused by M_w7.9 Wenchuan earthquake, May 12, 2008. Sci China Ser D-Earth Sci, 2009, 52: 593–601

61 Christensen N I. Poisson's ratio and crustal seismology. J Geophys Res, 1996, 101: 3139–3156

62 Zhou Y S, He C R. The rheological structure of crust and mechanics of high-angle reverse fault slip for Wenchuan M_s8.0 earthquake (in Chinese). Chinese J Geophys, 2009, 52: 474–484

63 Shan B, Xiong X, Zheng Y, et al. Stress changes on major faults caused by 2013 Lushan earthquake, and its relationship with 2008 Wenchuan earthquake. Sci China Earth Sci, 2013, doi: 10.1007/s11430-013-4642-1